RESEARCH ARTICLE   OPEN ACCESS

A Study of Anodic Voltage Drop in Aluminum Reduction Cell by Finite Element Analysis

Mahmoud A.Aly[1], Mohamed M. Ali[1]and A. A. Atlam[2]

1- Mining and PetroleumEngineering Dept., Faculty of Engineering, Al-Azhar University, Qena- Egypt.
2- Mining and PetroleumEngineering Dept., Faculty of Engineering, Al-Azhar University, Cairo- Egypt.

Abstract
Aluminum extraction has a very high energy consumption process, so reducing energy consumption is one of the most important roles in aluminum reduction cell design. The good path to achieve this goal can be made by voltage savings at the anode assembly.

The aim of this work is todevelop3D thermo-electrical finite element model and validate based on actual temperature measurements and electrical calculations for the anode assembly. The model is used to estimate the temperature distribution and the anodic voltage drop over the anode assembly and to suggest alternative design modifications to reduce the anodic voltage drop.

The effect of changing in stub diameter and chemical composition of cast iron on anodic voltage drop were studied. The findings indicated that the effect of stub diameter is more effective as compare with the changing in cast iron composition.

I.   Introduction

The best attempt to extract aluminum has been achieved by Hall and Héroult cell as shown in Figure1. This process produces the liquid aluminum by the electrolytic reduction of alumina (Al_2O_3) dissolved into an electrolyte consisting primarily of cryolite (Na_3AlF_6).

This process is a high-energy consumption process, so energy consumption is actually a better measure of cell performance, because it includes both cell voltage and current efficiency. The most modern aluminum smelters move close to 13 kWh to produce 1 kg of aluminum, and the world average value for the direct current energy consumption now may be close to 14 kWh/kg Al[1], while the theoretical energy consumption is only 6.34 kWh/kg Al at 977 °C[2].The best way to improve the power efficiency of this technology can be achieved by saving voltages at anode assembly [3-8].

In aluminum reduction cell, the anode assembly consists of aluminum rod connected to steel yoke which comprising into many steel stubs. The steel stubs are inserted into predefined holes in the anode carbon block, and the gap between carbon anode and steel stubs is filled with liquid cast iron.

After sealing, the cast iron shrinks significantly as it cools, creating an air gap that is detrimental to current efficiency of the new anode when it is installed in the cell. This air gap is critical to anode performance, as it increases the contact resistance of the anode connection increased. Also the anodic voltage drop influenced by cell operational factors such as stub deterioration[5].

Typical voltage drop in the anode was about 300mV which represented about 7~9 percent of the overall cell voltage[9]. There is much practical experience ega the red with respect to design and constructional changes aimed to reduce cell voltage in aluminum reduction cell[3, 4, 10, 11].

The first 3D thermo-electric half anode model was built in 1984 using ANSYS 4.1[10]. The modification of anode assembly design can reduce the anode voltage drop and the voltage drop is proportional to the height of the anode carbon block[4].Also other 3D finite element model was used to estimate the voltage drop, and found that the voltage drop increases with decrease the stub diameter[3].Also increasing the stub diameter has many benefits, such as lower electrical resistance and less likely to be damaged [4].The impact of stub deterioration and yoke stiffness on the anode connection was studied using 3D finite element model[11].

In this study a finite element model is adopted and used to solve the 3D thermo-electrical anode model. Different stub diameters and various compositions of cast iron were studied to reach to the best conditions for these parameters.
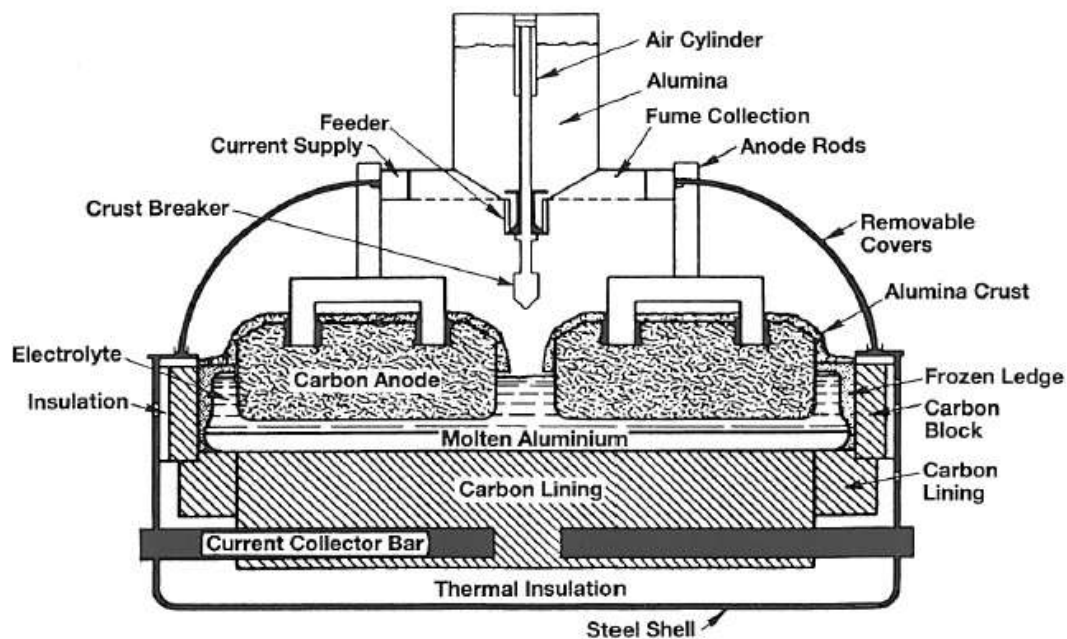
Figure1-Hall-Héroult cell with prebaked anodes (cross section)[2]

II. Thermal – electrical model

All geometry parts (aluminum rod, steel stubs, cast iron thimbles and anode carbon block) were developed by ANSYSacademicstudentv16.1workbench, but assembly together by using SolidWorks.

The following equations have been used to solve the coupling between thermal and the electrical fields:

1-   Temperature dependent electric conductivity $\sigma = \sigma\,(T)$

2-   Temperature dependent apparent current density

$$Y = \left(\sum_{n=0}^{5} b_n (DoD)^n \right) e^{C_1 \left(\frac{1}{T_{ref}} - \frac{1}{T} \right)}$$

(1)

3-   Temperature dependent equilibrium voltage (V)

$$U = \left(\sum_{n=0}^{5} a_n (DoD)^n \right) - C_2 (T - T_{ref})$$

(2)

4-   Joule heating as a volumetric source term for thermal energy equation

$$S_{joule} = \frac{i^2}{\sigma} = \frac{\sigma^2 \nabla^2 \phi}{\sigma} = \sigma \nabla^2 \phi$$

(3)

5-   Reaction heating as a volumetric source term for thermal energy equation

$$S_{echem} = j \cdot [U - (\phi_c - \phi_a)] \frac{A}{Vol}$$

(4)

The simulation model is based on the geometry of the anode assemblyat Egyptalum. The anode assembly consists of an aluminum rod, four steel stubs, cast iron thimble and anode carbon block as shown in Figure2.

The base model dimensions for anode carbon block are 1650 mm length, 720 mm width and 600 mm height. The four stubs are in diameter 130 mm, and offset 360 mm from each other, the stubs have height of 355 mm. The stub holes are 195 mm in diameter. The aluminum rod is 160 mm length, 158 mm width, and 2500 mm height. To simulate the flutes in the stub holes, 6-flutes configuration was chosen. Each flute has a square shape with sides of 20 mm, and an angle of 15⁰[12].

The cast iron used to establish the connection between steel stubs and anode carbon block is high phosphorus gray iron (HPGI).

The meshing process is fully automatic in ANSYS workbench, with focus on applying a fine mesh at locations where the temperature is expected to be high. The overall number of elements and nodes of the model are 60768 and 133159 respectively
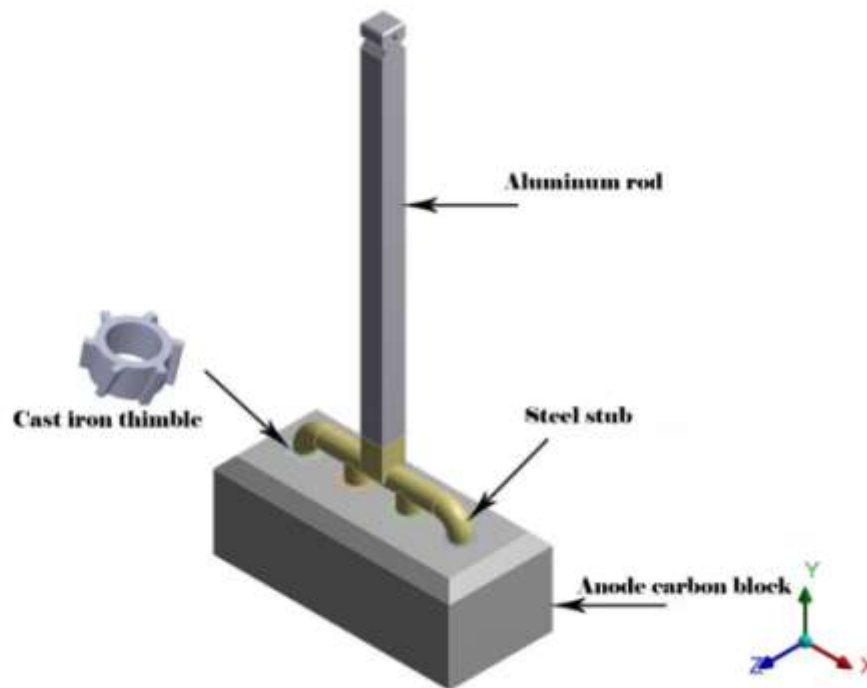
Figure2Anodeassembly model.

III. Material properties

Each part of anode assembly has different material properties. Most of the material properties have been found in elsewhere [5,7, 12-14], and from the data collected from Egyptalum.

Initial air gap

The air gap was happened during the rodding process, where the anode connection is established as hot cast iron is poured into the annular space between stub and carbon anode established by using pair of equations[15]:

$$S_{gap} = \gamma s + (t - {}_\gamma s) * \alpha_{cI} * (T_{cI} - T_0) \qquad (5)$$

$$\gamma s = r_s * \alpha s * (T_s - T_0) \qquad (6)$$

$$t = \frac{dsh}{2} - r_s \qquad (7)$$

By using equations (5-7),the initial gap between cast iron/carbon is estimated as shown in Figure 3.The air gap decreases as the stub diameters increase at different positions of cylindrical portion, the tip of flutes and the sides of flutes. This means that the contact resistance of the anode connection increase.
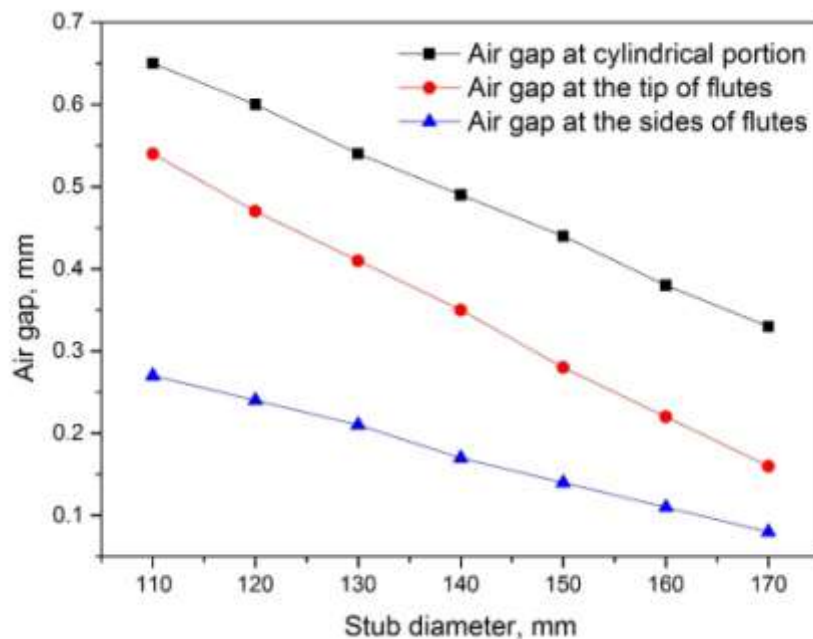
Figure 3Estimationof the air gap for various stub diameters.

Thermal boundary conditions

The top heat is transferred from the bath region under the anode carbon block in three main ways:

- The first is transfer from the anode carbon block to the rest of anode assembly (steel stubs and aluminum rod) by conduction and convection from anode carbon block surface to the air inside the superstructure.
- The second mechanism is conduction from steel stubs to the aluminum rod and then convection to the air inside the super structure.
- The third mechanism is convection from aluminum rod to the air inside the super structure.

The convective heat transfer coefficient in this workbased on Pr, Gr, Ra and Nu equations is calculatedfor each part of anode assembly and is ranged between 4.8 and $11.11 W/m^2.k$. These values is confirmed with the data published in elsewhere, where the heat transfer coefficients into anode assembly was ranged between 5 and 15 $W/m^2.k$[16, 17].

These coefficients are be applied in all thermal analysis modeltaking into account the temperature of $960°C$ at the bottom of the anode carbon block as bath temperature , and $150°C$ at the top of an aluminum rod based on actual cell measurements.

A condition of periodicity is assumed between the outer anodes and central anode in the cell. Therefore, heat transfer between these anodes is negligible and adiabatic condition in apply on these surfaces[3].

Electrical boundary conditions

To simulate the electrical conditions, more than one condition will be applied in this model:

a- Zero potential is applied on the bottom surface of the anode carbon block (Dirichlet boundary condition) to simplify the calculations. Although in practice, potential at the bottom surface of the anode carbon block is not zero[5, 7, 9].

b- A current of 8750 A is applied at the top surface of the aluminum rod based on cell current of 210 kA and 24 anodes per cell.

IV.   Experimental work

Four cells were selected to do the thermal measurements at the different positions on the anode assembly in figure illustrated in Table 1.

These measurements were done using Infrared thermometer and used to validate the thermal model.

The average measured temperatures for the aluminum rod, steel yoke, steel stubs and anode carbon block are 169, 340, 420 and 490°C respectively. The temperature values increase as move down towards the bottom of the anode.

For the electrical model, the voltage drop through the anode assembly is calculated in this work and found nearly 395 mV.

Table 1Temperature measurements at different locations on the anode assembly.

Anode carbon block NO.		10		8	
Read Title	Read No.	Cell 603	Cell 604	Cell 633	Cell 634
Aluminum rod	A1	296	250	272	280
	A2	157	164	179	176
Steel yoke	S5	370	350	380	365
	S6	372	365	385	370
	S7	307	294	330	310
Steel Stubs	S1	420	428	440	415
	S2	405	415	420	407
	S3	405	412	425	410
	S4	422	430	443	417
Anode carbon block	C1	420	450	489	400
	C2	500	495	544	506
	C3	510	550	571	496
	C4	535	490	552	516
	C5	418	436	470	450
	C6	509	484	540	490
	C7	497	510	545	554
	C8	428	434	465	440

(Temperature, °C)
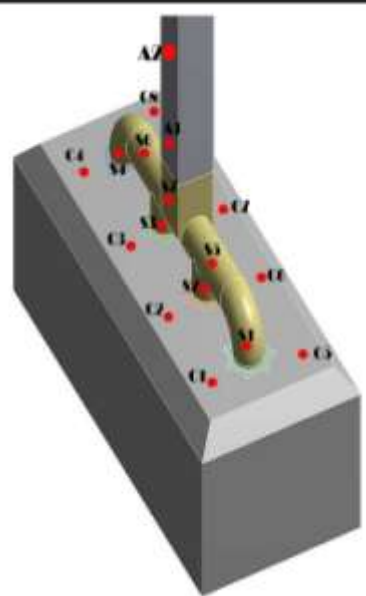
V. Base model validation

Validation of the base model is the most important step in studying the mathematical modeling, where using an unvalidated cell model can be very misleading[18].The thermal and electrical results for the base model are represented in Figure 4 (a and b).The temperature values obtained from the thermal model is close to measured values as shown in Table2, where the difference andthe percentage error between thermal model results and measured temperature values at anode assembly don't exceed 10%, and these values are considered acceptable to validate the model.

      (a)   (b)
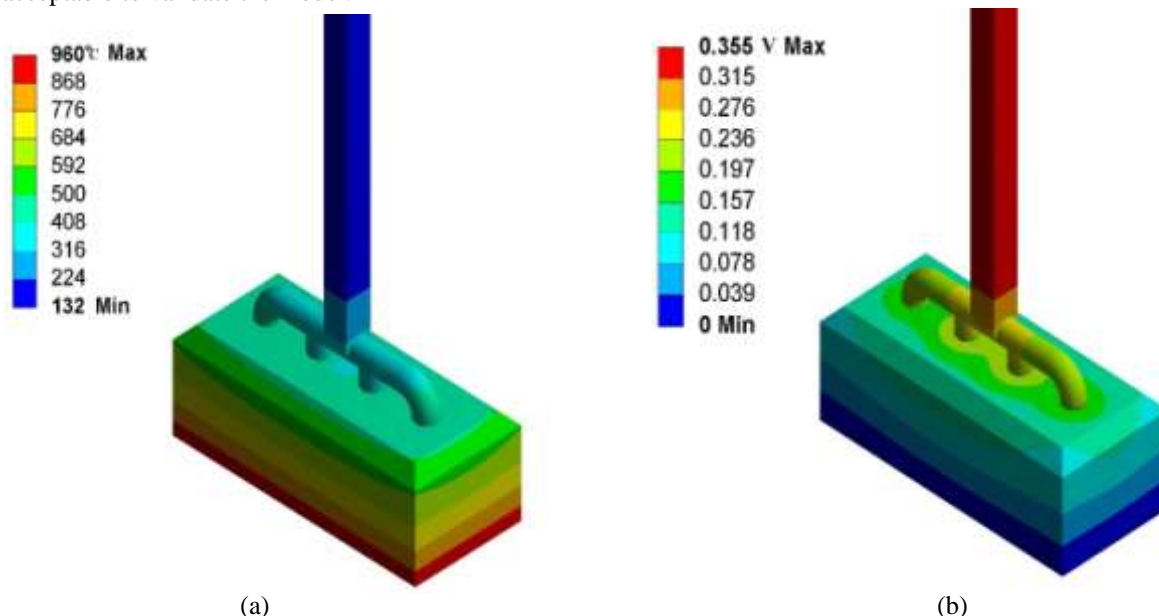
Figure 4 Thermal distribution, ^{o}C (a) and electricalpotential, V(b)for the base model.

Table2Comparison between thermal model temperatures andmeasuredtemperature at different locations on the anode assembly.

Position \ Item	Modelled temp.,˚C	Measured temp.,˚C	Percentage difference %
A-r	169	160	5
S-y	340	370	8
S-b1	425	462	8
S-b2	411	452	9
S-b3	413	452	8
S-b4	428	463	7
A-c	490	524	6
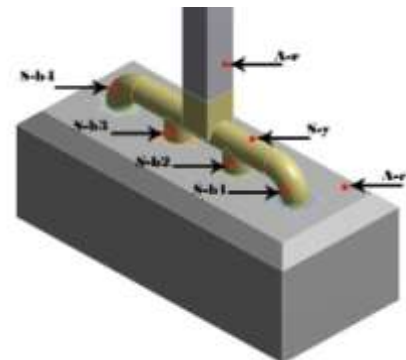
- For the electrical model the voltage drop over the anode assembly is about 355 mV and this result fits well with the calculated values with differenceof about 10%.

Cases examined

In this work, two cases were studied:-

-In the first case, the designed stub diameter of 130mm was changed to different stub diameters of 110, 120, 140, 150, 160 and 170 mm representing different stages of stub deterioration as stub diameters 110 and 120mm and size enlargement of the stub diameter in the rest cases. When an anode is set in the cell, steel stubs and cast iron expand creating pressure to achieve a good electrical contact. This was with the intention to increase the stub dimension, which could lead to anode voltage saving [3-5].

- In the second case each of the stub configuration models were studied using different composition of cast iron (ductile cast iron).

These cases were solved and compared with respect to the temperature and voltage distribution in this work. The boundary conditions are fixed for all case studies as do in the base model.

VI. Results and discussion

First case: Deterioration and enlargement of stub diameter

Different stub diameters of 110, 120, 140, 150, 160 and 170 mm -representing different stages of deteriorationand enlargement of the stub diameter- were studied. Two cases of stub diameters configurations (110 and 170 mm) wereillustrated in Figure 5.Little differences in temperature distributionbetween the two cases and this difference areappeared around the steel stubs locations. This increase in temperature may be related to increase the contact pressure between the steel stub and anode carbon block.

(a)   **(b)**
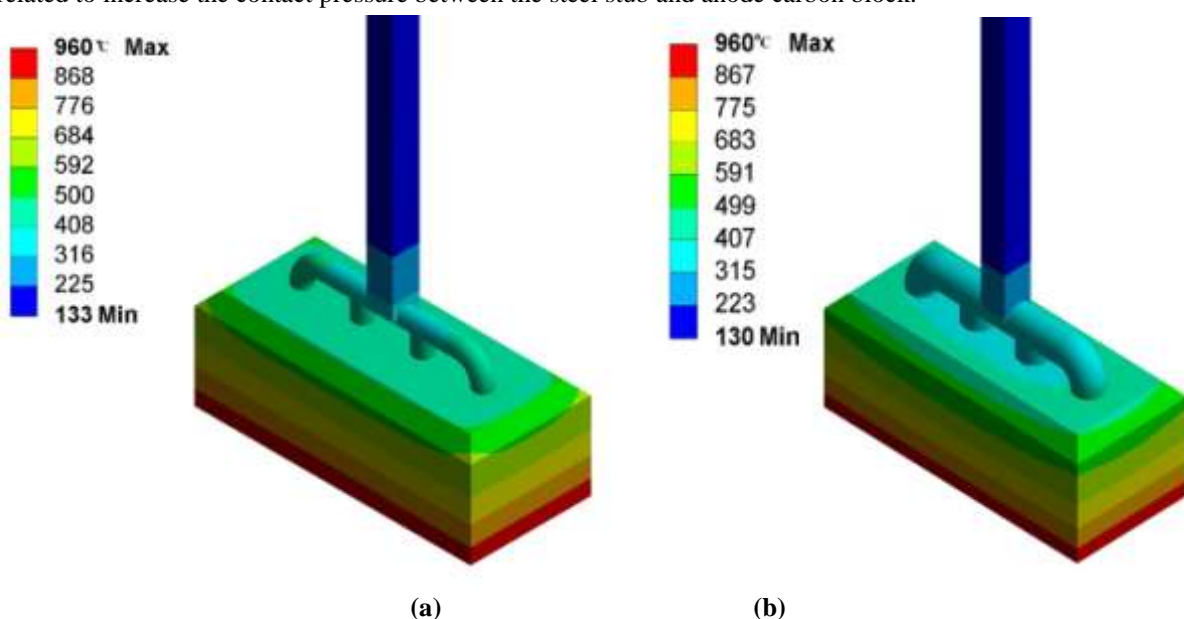
Figure 5 Temperature distribution model for (a) 110mmand (b)170mm stub diameter.

The average temperature of each part of anode assembly was illustrated in Figure6 for different models as function of stub diameter. It can be seen that the temperature decreases with increasing in the stub diameter for all regions. The aluminum rod region represents the lowest temperature values while the upper parts of anode carbon block represent the highest temperature values.

Comparison the temperatures variations with increasing the stub diameter illustrated low influence in the aluminum rod and anode carbon block temperature, and high influence on the cast iron and steel stub temperature. The temperature values in these regions depend on the size of an air gap developed at these locations. The increased in an air gap gives decreased in the contact pressure and hence decreased the actual contact area, which causes increased in ohmic heat generation and hence higher temperatures at these parts.
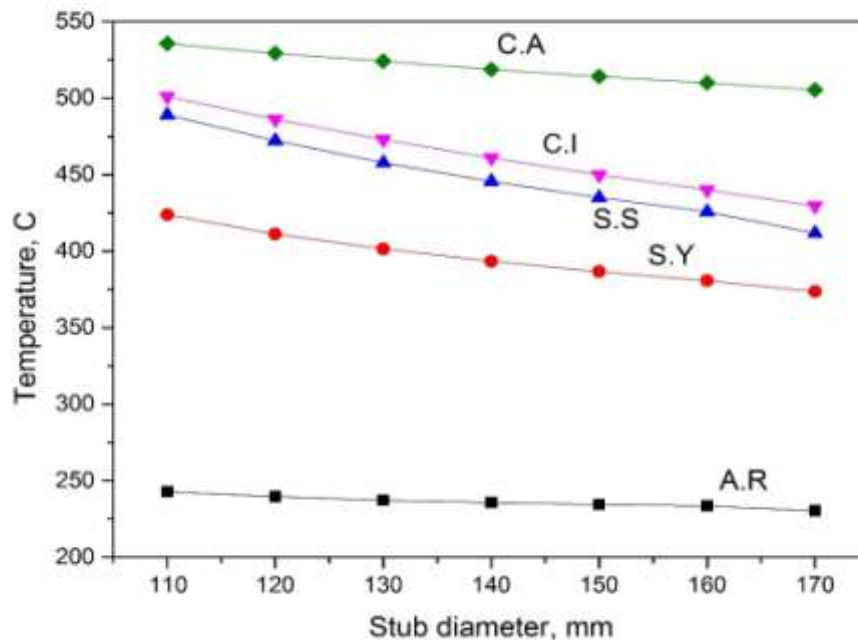
Figure 6 Average temperatures in each part of the anode assembly as function of stub diameter.

Figure 7represents the voltage drop at two different stub diameters (110 and 170 mm).As stated in the boundary conditions section, the bottom of the anode carbon block has beenset to zero voltage. Thus, it can be concluded that the electric potential at the top of the aluminum rod, where the electric current is imposed to the model represents the total voltage drop of anode assembly.

The central stubs (numbers 2 and 3) are appeared to have the highest voltage drop of all stubs in each configuration, and this is due to that the electric current move through the shortest possible path to the bottom of the anode carbon block.

The results in this work show that the anodic voltage drop decreases with increasing the stub diameter and this is agreed with published data in elsewhere[4, 5, 7, 9] but with difference in voltage drop values from one to another reference [4].

Figure 8, shows that the maximum voltage drop decreases with increases the stub diameter, it can be seen that, about 10 m volt can be reduced for each increase of stub diameter by 10 mm. But the cast iron thickness decreases which may cause falling the anode carbon block in the bath, so choosing the best stub diameter based on study the mechanical behaviour of the anode assembly. The relation between different stub diameters and maximum principle stress based on the thermo-electro - mechanical coupling is illustrated in Figure 9. It can be seen that the stub diameter of 140 mm gives the best conditions. The calculated stress of 2.4 MPa is only 2 % of available strength. Therefore if the steel stub temperature is about 500°C, the stress of 2.4 MPa will be quite safe. More detailed about the solving procedures of the thermo-electro- mechanical finite element model of the anode assembly will be appeared in another paper.
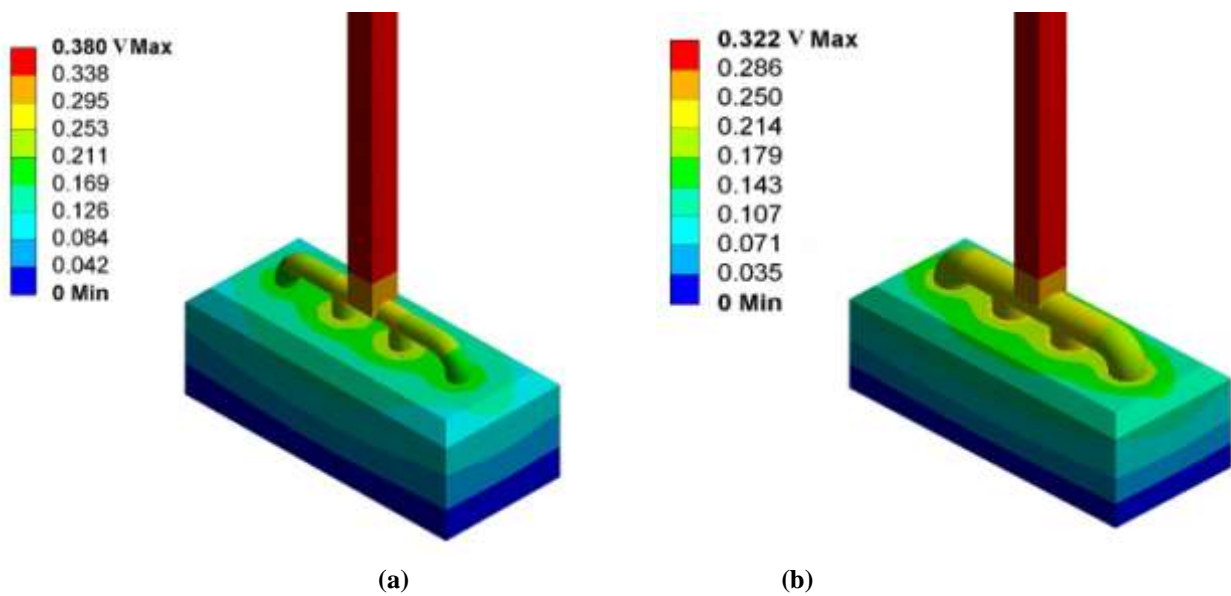
(a) **(b)**
Figure 7 Voltage distribution (ᵒC) for (a) 110mmand (b) 170mm stub diameter
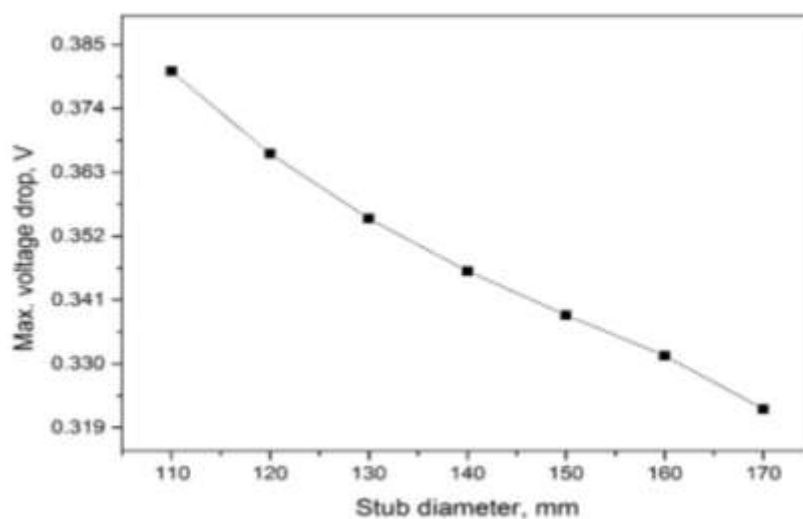
Figure 8 Maximum voltage drop with different stub diameters
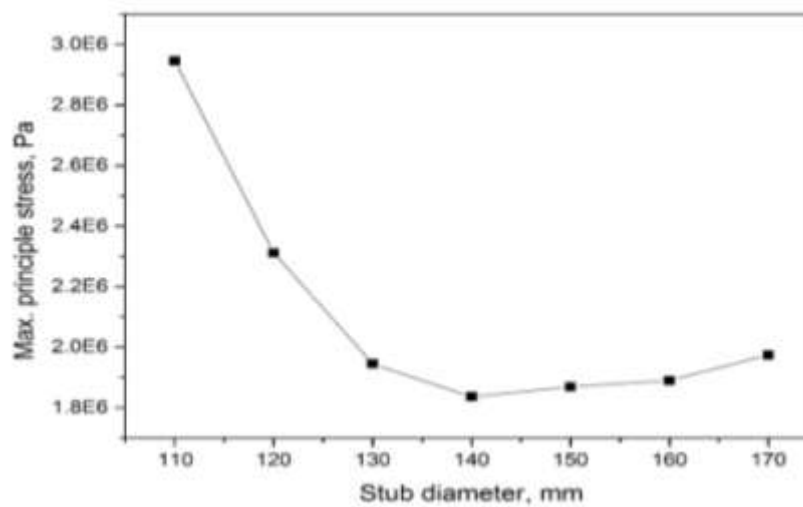
Figure 9 Relation between stub diameter and maximum principle stress

Second case: Different cast iron composition

The simulation with different stub diameters (110,120, 140, 150,160 and 170 mm) was repeated with different composition of cast iron (ductile cast iron). Figure10 shows the predicted average temperature of each part of anode assembly.The general trend in this figure is confirmed with the result of HPGI with little decrease in the temperature of ductile cast iron.

Figure 11 shows the cast iron temperature for both cast iron compositions as a function of the stub diameter. The temperature is little lower for configuration with HPGIas compared withductile cast iron.
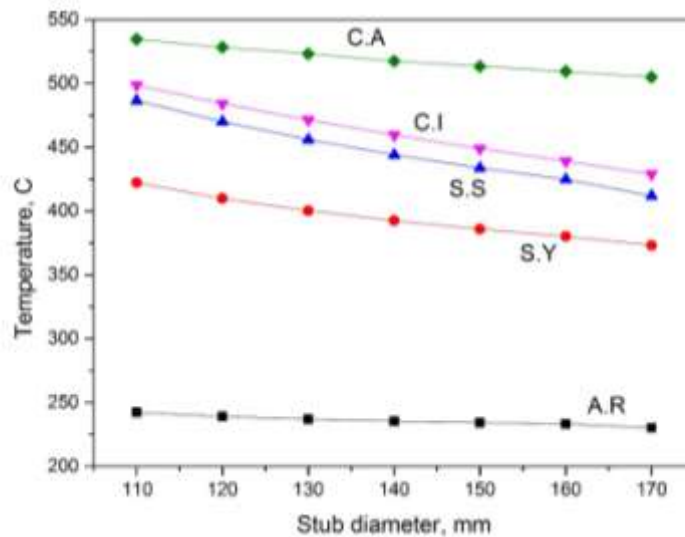
Figure 10 Average temperatures in each part of anode as function of stub diameter with ductile cast iron
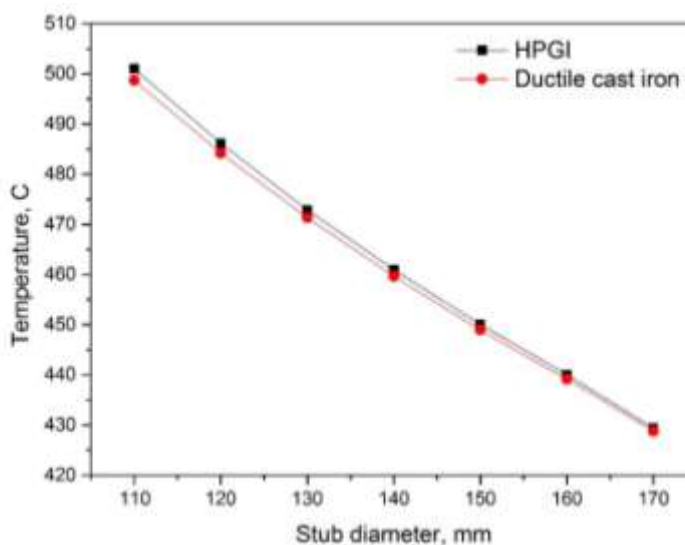
Figure 11Cast iron temperature for both cast iron compositions as afunction of different stub diameters.

Figure12 illustrates the maximumvoltage drop for both cast iron compositions as function of stub diameter.The voltage drop for anode assembly is decreased for ductile cast iron as compared with HPGI. The maximum anodic voltage drop is lower in ductile cast iron as compared with HPGI for all stub diameters by about 3 m volt. Voltage drop reducing in ductile cast iron is related with the process of production, where the ductile cast iron is produced by introducing asmall amount of magnesium or cerium into the molten iron.These additions catalyze the decomposition of carbon into spheroids and not flakes, and hence contact pressure of ductile cast iron [19, 20].
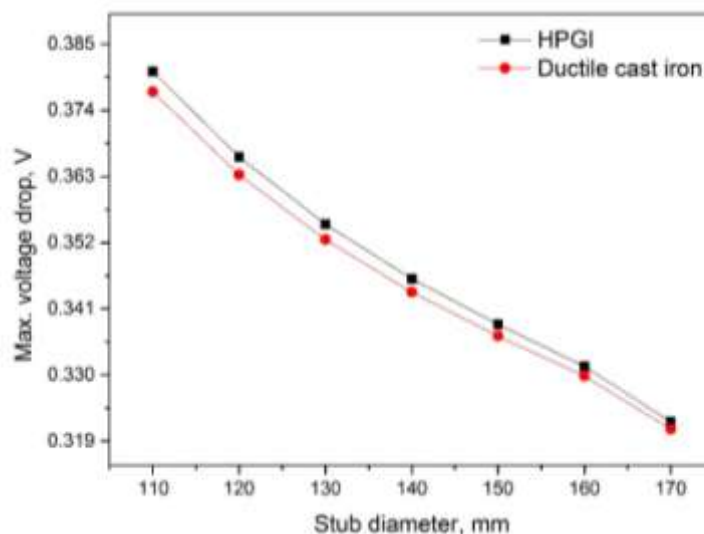
Figure 12Maximum voltage drop as function of stub diameter for both cast iron compositions

VII. Conclusion

Good agreement between the model predictions and the thermal measurements and the electrical calculations stresses the validity of the 3D thermo-electrical anode model.

Air gap has important effect of the establishment of the contact pressure and the voltage drop in the model. The initial air gap was found inversely proportional to stub diameter.

The model results show that the stub diameter and composition of cast iron have affected onanodic voltage drop. About 10 mvolt can be reduced for each increase of stub diameter by 10 mm. Also about 3m volt can be saved by using the ductile cast ironinstead of HPGI forthe stubanode connection.

The anode assembly configuration with 140 mm stub diameter and ductile cast ironwas given the best results for lower voltage dropbased onour primary study of the thermo-electro-mechanical model.

Acknowledgment

References

[1] H. Kvande and P. A. Drabløs, "The aluminum smelting process and innovative alternative technologies," Journal of Occupational and Environmental Medicine, vol. 56, p. S23, 2014.
[2] K. Grjotheim and H. Kvande, Introduction to aluminium electrolysis: Understanding the Hall-Héroult process. Düsseldorf: Aluminium-Verlag, 1993.
[3] H. Fortin, M. Fafard, N. Kandev, and P. Goulet, "FEM analysis of voltage drop in the anode connector assembly", TMS Light Metals, vol. 1, pp. 1055-1060, 2009.
[4] W. Li, J. Zhou, and Y.-w. Zhou, "Numerical analysis of the anode voltage drop of a reduction cell", TMS Light Metals, pp. 1169-1171, 2009.
[5] S. Beier, "A study of an anode assembly with focus on the anode connection used in aluminium reduction cells," Msc., 2010.
[6] H. Fortin, N. Kandev, and M. Fafard, "FEM analysis of voltage drop in the anode connector induced by steel stub diameter reduction," Finite Elem. Anal. Des., vol. 52, pp. 71-82, 2012.
[7] E. Jeddi, "Numerical study of anodic voltage drop in the Hall-Héroult cells by finite element method", Msc, QUÉBEC University, 2013.
[8] E. Efficiency, "US Energy Requirements for Aluminum Production," 2007.
[9] H. Fortin, "Modélisation du comportement thermo-électro-mécanique de l'anode de carbone utilisée dans la production primaire de l'aluminium," M.Sc, Université Laval, 2009.
[10] M. Dupuis, "Using ANSYS to model aluminum reduction cell since 1984 and beyond," in Proceedings of the ANSYS 10th International Conference, 2002.
[11] S. Beier, J. J. Chen, H. Fortin, and M. Fafard, "FEM analysis of the anode connection in aluminium reduction cells," TMS Light Metals, pp. 979-984, 2011.

[12] M. Agour, "Castironforanodefixationcollars," M.Sc, Mining &Metallurgical Engineering, Al-Azhar University, Cairo, 2011.

[13] A. Handbook, "Volume 1 Properties and selection: irons, steels and high performance alloys, 1990, ASM International, The Materials Information Company, United States of America," ISBN 0-87170-377-7.

[14] S. Wilkening and J. Côté, "Problems of the stub-anode connection," Essential Readings in Light Metals: Electrode Technology for Aluminum Production, Volume 4, pp. 534-542, 2007.

[15] D. Richard, P. Goulet, O. Trempe, M. Dupuis, and M. Fafard, "Challenges in stub hole optimisation of cast iron rodded anodes," Light metals., vol. 2009, pp. 1067-1072, 2009.

[16] H. Abbas, "Mechanism of top heat loss from aluminium smelting cells," PhD, AucklandUniversity, 2010.

[17] D. Gunasegaram and D. Molenaar, "A fully coupled thermal-electrical-mechanical transient FEA model for a 3D anode assembly," Light Metals 2013, pp. 1341-1346, 2013.

[18] M. Dupuis, "Process simulation," TMS Course on Industrial Aluminum Electrolysis, 1997.

[19] A. K. Chakrabarti, "Casting technology & cast alloys," Prentice hallof India privatelimited, New Delhi, (2005).

[20] R. Elliot, "Cast iron technology," Butterworth, London, (1988).

Symbols

A	= Local surface area of the interface
A.R	= Aluminum rod
C_1, C_2	= Two additional model coefficients
C.A	= Anode carbon block
DOD	= Depth of discharge
dsh	= Stub hole diameter, mm
Gr	= Grashof number
h	= Convective heat transfer coefficient, $w/m^2.k$
HPGI	= High phosphorous gray iron
I	= Current
J	= Apparent current density
Nu	= Nusselt number
Pr	= Prandtl number
Ra	= Rayleigh number
r_s	= Stubradius, mm
S_{echem}	= Reacting heat
S_{gap}	= Air gap size at T_0, mm
Sjoule	= Joule heat
S.S	= Steel stub
S.Y	= Steel yoke
T_0	= Ambient temperature, $^\circ$C
T_{cI}	= Temperature of cast iron, $^\circ$C
T_s	= Temperature of steel stub, $^\circ$C
t	= Stub hole gap, mm
U	= The intercept of V at I=0
V	= Voltage
VOL	= Volume of the computing cell
Y	= The inverse of the slope of the V-I curve.
αs	= Thermal expansion coefficient of steel, $\frac{1}{K}$
α_{cI}	= Thermal expansion coefficient of cast iron, $\frac{1}{K}$
γs	= Change in radius of the steel stub, mm
σ	= Electric conductivity
$\phi_c - \phi_a$	= Separator interface between cathode and anode